

# Some Physical Layer Issues of Wide-band Cognitive Radio Systems

Haiyun Tang  
ADAPTRUM, INC.  
2029 STIERLIN CT., STE. 100  
MOUNTAIN VIEW, CA 94043  
Email: haiyun@adaptrum.com

**Abstract**—Recent study by FCC Spectrum Policy Task Force (SPTF) found that while the available spectrum becomes increasingly scarce, the assigned spectrum is significantly underutilized. Cognitive radio technology holds the key promise to solve such problems. In this paper, we investigate some physical layer issues of wide-band cognitive radio systems. Specifically, we discuss the physical layer signal structure to support flexible operations required by wide-band cognitive radios. We analyze the performances of generalized power sensing and waveform sensing. And we study the adjacent channel interference mechanisms focusing on the interference caused by time-domain signal truncation.

## I. INTRODUCTION

Recent study [1] by FCC Spectrum Policy Task Force (SPTF) found that while the available spectrum becomes increasingly scarce, the assigned spectrum is significantly underutilized. The situation is especially acute in lower frequencies where the radio signal propagation characteristics are more favorable. The imbalance between spectrum scarcity and spectrum underutilization is especially inappropriate today, when significant amount of radio spectrum is needed to provide ubiquitous wireless broadband connectivity.

A radio technology that holds the key promise to solve such problems is the *cognitive radio* [2] – a radio that is capable of dynamically sensing and locating unused spectrum segments in a target spectrum pool and communicating using the unused spectrum segments in ways that cause no *harmful* interference to the primary users of the spectrum [3], [4].

Cognitive radio is considered as a spectrum sharing technology like ultra-wide-band [5]. The key difference is that while the UWB signal spectrum overlaps with the primary user signal spectrum, a cognitive radio's signal spectrum resides solely in the unused spectrum segments or spectrum holes. As a result, a cognitive

radio device may transmit high signal power than a UWB device, as long as it can correctly identify the unused spectrum segments and the spectral leakage due to its signal transmission doesn't substantiate harmful interference in the primary user spectrum bands.

While UWB technologies usually apply to short-range communications due to transmission power limitations, cognitive radio technologies may be used in longer-range communications for applications like broadband wireless access. Furthermore, the ability of cognitive radios to identify and utilize the unused spectrum segments allows them to coexist with legacy radio systems, improving spectrum utilization without harming the primary users.

Three key aspects of a cognitive radio are:

- Sensing – A cognitive radio must be able to identify the unused spectrum segments.
- Flexible – A cognitive radio must be able to change signal frequency and spectrum shape to fit into the unused spectrum segments.
- Non-interfering – A cognitive radio must not cause harmful interference to the primary users.

This paper investigates these aspects of the cognitive radio system from a physical layer perspective. Specifically, Section II discusses the physical layer signal structure to support flexible operations required by wide-band cognitive radio systems. Section III analyzes general forms of power-based sensing and waveform-based sensing. Section IV studies interference to the primary users due to adjacent channel leakage mechanisms, focusing on the adjacent channel leakage due to time-domain signal truncation.

## II. SYSTEM CONSIDERATION

If a target primary user spectrum has fixed channelization, e.g. the TV bands, a wide-band cognitive radio system may use either time-based or frequency-based signals. When the target primary user spectrum doesn't

support fixed channelization, frequency-based signals are preferred, because it is difficult to dynamically generate a time-based signal whose spectral waveform can fit into arbitrarily-sized unused spectrum segments. From this perspective, we believe Orthogonal Frequency Division Multiplex (OFDM) is the ideal signal structure for wide-band cognitive radio systems. OFDM divides the target spectrum into narrowband subchannels and the signal values are modulated on the subchannels in frequency domain. Interference to the primary users is avoided by simply nullifying the subchannels in the occupied spectrum segments and modulating only the subchannels in the unused spectrum segments. With a sufficient number of subchannels, an OFDM-based cognitive radio system can operate efficiently in any target primary user spectrum regardless of its channelization scheme.

An OFDM-based cognitive radio system is also theoretically optimal since, in the limit of infinite number of subchannels, it allows to achieve the Shannon capacity in a fragmented primary user spectrum, i.e.

$$C = \int_{\Omega} \frac{1}{2} \log_2 \left[ 1 + \frac{G(f)S_0}{N_0} \right] df \quad (1)$$

where  $\Omega$  is the collection of unused spectrum segments;  $G(f)$  is the channel power gain at frequency  $f$ ;  $S_0$  and  $N_0$  are the signal and noise power per unit frequency respectively [6]. An OFDM-based system has other advantages including robust against multipath delay spread (using the guard interval or cyclic prefix), no need for complex time-domain equalization, insensitive to sampling time drift (and thus no need for complex sampling time tracking), and easy integration with multi-antenna algorithms [7].

### III. SENSING

A cognitive radio uses sensing to determine spectrum availability. In general, we can separate physical layer sensing methods into two categories: power-based sensing methods and waveform-based sensing methods. Since any information-bearing signal has finite signal power, one usually resorts to power-based sensing if nothing else is known about the target primary user signal. Power-based sensing methods, however, are prone to false detections and usually work poorly when the target signal SNR is low. When the target signal contains known signal patterns, e.g. DTV or NTSC signals, waveform-based sensing can be performed, which usually gives far better performance than power-based sensing in terms of sensing sensitivity and reliability.

#### A. Power-based sensing

Power-based sensing can be performed in both time domain and frequency domain. To measure the signal power in a particular frequency region in time domain, a bandpass filter is applied to the target signal and the power of the signal samples (after the filter) is then measured. To measure the signal power in frequency domain, the time-domain signal is transformed to frequency domain using FFT and the combined signal power over all frequency bins in the target frequency region is then measured.

For either case, we consider the received signal of the form

$$y(n) = x(n) + z(n) \quad (2)$$

where  $x(n)$  is the target signal;  $z(n)$  is the white Gaussian noise; and  $n$  the sample index in the case of time-domain sensing, or FFT symbol index in the case of frequency-domain sensing. For simplicity of derivation, we will assume the signal sample  $x(n)$ s are independent. Correlation among signal sample  $x(n)$ s, e.g. due to multipath channel memory effect, will only improve the sensing performance. Since the noise sample  $z(n)$ s are also independent, the received sample  $y(n)$ s are independent.

Consider using the following signal power sum as the power sensing metric:

$$S = \sum_{n=1}^{N_B} |y(n)|^2 \quad (3)$$

where  $N_B$  is the summing buffer size. Note that  $|y(n)|^2$  is a sequence of independent and identically distributed (IID) random variables with mean and variance

$$E[|y(n)|^2] = \mu, \quad E\left[\left\{|y(n)|^2 - \mu\right\}^2\right] = \sigma^2 \quad (4)$$

When  $N_B$  is large, using central limit theorem [8], the sensing metric  $S$  in (3) can be approximated as a Gaussian random variable with mean and variance

$$\mu_S = N_B \mu, \quad \sigma_S^2 = N_B \sigma^2 \quad (5)$$

When there is no signal present, i.e.  $x(n) = 0$ , the sensing metric is:

$$S = S_0 = \sum_{n=1}^{N_B} |z(n)|^2$$

When there is signal present, the sensing metric is:

$$S = S_1 = \sum_{n=1}^{N_B} |y(n)|^2$$

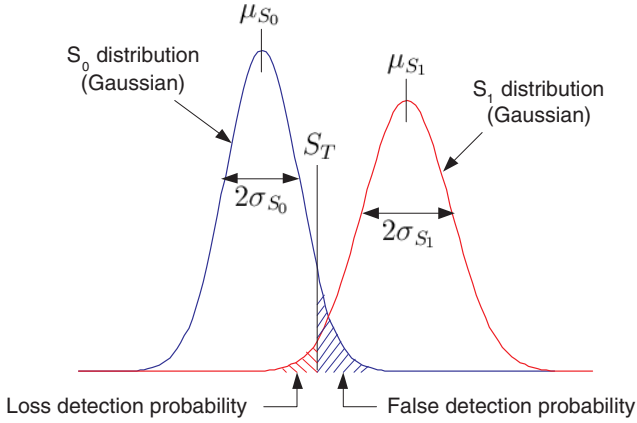


Fig. 1. Illustration of power sensing false detection probability versus loss detection probability.

Figure 1 shows the distributions of  $S_0$  and  $S_1$ , which are Gaussians. The signal presence is determined by comparing the measured sensing metric  $S$  against certain sensing threshold  $S_T$ . Referring to the figure, false detection probability (PFD) is the probability that  $S > S_T$  when there is no signal present and the loss detection probability (PLD) is the probability that  $S < S_T$  when there is signal present. The tradeoff between PFD and PLD leads to the optimal sensing threshold  $S_T$ , when the PFD is equal to the PLD.

We define the sensing error floor (SEF) as the PFD (or PLD) at the optimal threshold. Since both PFD and PLD are Gaussian tail integrations that can be expressed in terms of the Q function [8]:

$$\text{PFD} = Q\left(\frac{S_T - \mu_{S_0}}{\sigma_{S_0}}\right), \quad \text{PLD} = Q\left(-\frac{S_T - \mu_{S_1}}{\sigma_{S_1}}\right) \quad (6)$$

the optimal sensing threshold  $S_T$  is found by equating the arguments of the above Q functions

$$\frac{S_T - \mu_{S_0}}{\sigma_{S_0}} = -\frac{S_T - \mu_{S_1}}{\sigma_{S_1}} \Rightarrow S_T = \frac{\mu_{S_0}\sigma_{S_1} + \mu_{S_1}\sigma_{S_0}}{\sigma_{S_0} + \sigma_{S_1}} \quad (7)$$

Using  $S_T$  expression (7) in the PFD (or PLD) expression in (6), we obtain the sensing error floor

$$\text{SEF} = Q\left(\frac{\mu_{S_1} - \mu_{S_0}}{\sigma_{S_0} + \sigma_{S_1}}\right) \quad (8)$$

It can be shown, after some mathematical steps, the sensing error floor (8) can be expressed in terms of the signal-to-noise ratio and summing buffer size as:

$$\text{SEF} = Q\left(\sqrt{N_B} \frac{\text{SNR}}{1 + \sqrt{[\alpha - 1]\text{SNR}^2 + \text{SNR} + 1}}\right) \quad (9)$$

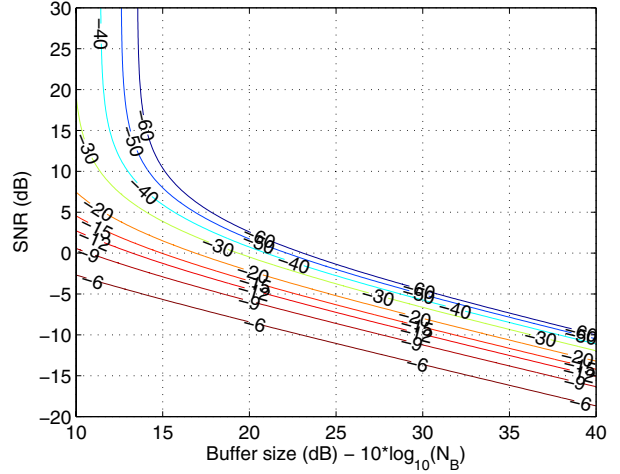


Fig. 2. Power sensing error floor contours under different SNRs and summing buffer sizes.

Here

$$\text{SNR} = E[|x(n)|^2] / E[|z(n)|^2] \quad (10)$$

is the nominal symbol SNR and

$$\alpha = E[|x(n)|^4] / \{E[|x(n)|^2]\}^2 \quad (11)$$

is an intrinsic parameter of the signal  $x(n)$  that relates its randomness. For example, for complex Gaussian signal,  $\alpha$  is 2. For constant-amplitude signals, e.g. BPSK, QPSK, and 8-PSK,  $\alpha$  is 1. For other types of signals,  $\alpha$  is between 1 and 2.

Figure 2 shows the sensing error floor (9) contours at different SNRs and summing buffer sizes, with  $\alpha = 2$  (Gaussian signal). Note that the error floor is expressed in dB units, e.g. -20 dB corresponding to 0.01. When  $\text{SNR} \ll 1$ , the argument of the Q function in (9) is approximated as

$$\sqrt{N_B} \frac{\text{SNR}}{2}$$

In other words, a linear decrease in SNR requires a quadratic increase in the buffer size  $N_B$  to maintain the same SEF. When  $\text{SNR} \gg 1$ , the argument of the Q function in (9) is approximated as

$$\sqrt{N_B} / \sqrt{\alpha - 1}$$

which is independent of SNR. Both of these trends are clearly shown in Figure 2.

### B. Waveform-based sensing

Power-based sensing is prone to false detections since it only measures signal power and could be easily triggered by unintended signals. The above discussion also shows that power-based sensing works poorly at low SNRs – when every 1 dB reduction in SNR requires 2 dB increase in the summing buffer size  $N_B$  to maintain the same sensing error. Both of these problems are addressed in waveform-based sensing, which is usually based on correlation with known signal patterns.

Waveform-based sensing is performed in time domain. We again use the received signal representation (2) and assume the signal  $x(n)$ s are independent. We assume the known time-domain signal pattern contains  $N_B$  signal samples. Consider the following waveform sensing metric:

$$S = \text{Re} \left[ \sum_{n=1}^{N_B} y(n)x^*(n) \right] \quad (12)$$

When there is no signal present, the sensing metric is

$$S = S_0 = \text{Re} \left[ \sum_{n=1}^{N_B} z(n)x^*(n) \right] \quad (13)$$

When there is signal present, the sensing metric is

$$S = S_1 = \sum_{n=1}^{N_B} |x(n)|^2 + \text{Re} \left[ \sum_{n=1}^{N_B} z(n)x^*(n) \right] \quad (14)$$

The sensing metric (12) can be approximated as a Gaussian random variable when  $N_B$  is large. Based on the similar arguments as before, the sensing error floor for waveform-based sensing is given by (8) with  $S_0$  and  $S_1$  given by (13) and (14) respectively.

It is possible to calculate the mean and variance of  $S_0$  as well as  $S_1$ , which can then be used in (8) to compute the sensing error floor for waveform-based sensing:

$$\text{SEF} = Q \left( \sqrt{N_B} \frac{\sqrt{\text{SNR}}}{\sqrt{(\alpha - 1)\text{SNR} + 1/2} + \sqrt{1/2}} \right) \quad (15)$$

Here  $\alpha$  is again given by (11). When  $\text{SNR} \ll 1$ , the argument of the Q function in (15) is approximated as

$$\sqrt{N_B} \sqrt{\frac{\text{SNR}}{2}}$$

In other words, linear reduction in SNR only requires linear increase in  $N_B$  in order to maintain the same sensing error floor. When  $\text{SNR} \gg 1$ , the argument of the Q function is approximated as

$$\sqrt{N_B}/\sqrt{\alpha - 1}$$

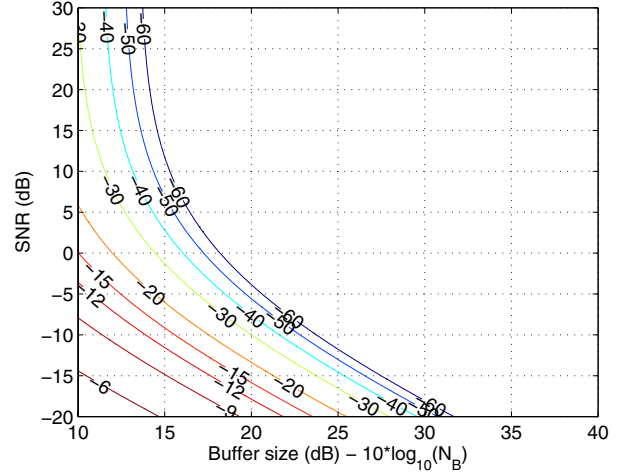


Fig. 3. Waveform sensing error floor contours under different SNRs and summing buffer sizes.

In other words, waveform-based sensing performs similarly as power-based sensing at high SNRs. Figure 3 shows the sensing error floor contours assuming  $\alpha = 2$ , i.e. Gaussian input  $x(n)$ .

The above approximation of the argument of the Q function at low SNR suggests  $N_B$  can be considered as the sensing gain (over the nominal symbol SNR). Note that when SNR increases, however, the structure of the signal as represented by  $\alpha$  will play a more important role in the SEF expression. Since the sensing gain  $N_B$  is equal to the length of the known signal pattern (in number of signal samples), a longer known signal pattern in the primary user signal will result in a better sensing performance. The above discussion didn't consider the effect of multipath, which tends to reduce the sensing gain by a factor equal to the normalized strength of the dominant multipath component, unless averaging is performed over adjacent multipath taps.

Figure 3 shows waveform-based sensing can achieve good performance even at low SNR as long as  $N_B$  is sufficiently large. In a practical shadowing environment, cognitive users may receive drastically different signal strengths (and thus SNRs) at different locations. An alternative to use a very large  $N_B$  to account for the worst-case shadowing scenarios is to allow sensing information sharing among local cognitive users so that sensing is performed collectively rather than individually to reduce the effect of shadowing [9].

#### IV. ADJACENT CHANNEL INTERFERENCE

To ensure successful operation, it is further required that cognitive radios must not cause harmful interference to the primary users when communicating using the unused spectrum segments identified through sensing. A likely cause of interference to the primary users is the adjacent channel leakage (ACL) as a result of cognitive user signal transmissions in bands that are adjacent to the primary user bands. Two mechanisms contributing to the adjacent channel leakage are signal time-domain truncation and transmission nonlinearity. Adjacent channel leakage can usually be controlled through careful system design.

##### A. Signal time-domain truncation

1) *Time-domain signals*: For a single-channel transmission system with fixed channel bandwidth, out-of-band emission can usually be controlled through either analog or digital filtering. For a wide-band system with signal transmission over discontinuous and arbitrarily-sized spectrum segments, limiting out-of-band emissions from individual spectrum segments through analog filtering may not be practical, since each spectrum segment may require a different analog filter with a different center frequency and bandwidth. Such filtering goal, however, can be achieved in digital domain through baseband pulse shaping.

While the available spectrum (identified through sensing) may consist of multiple spectrum segments, we will study the adjacent channel leakage by focusing on the out-of-band emission from a particular spectrum segment. The analysis should be easily extended to the general case of wide-band signal transmission over multiple frequency segments, where the adjacent channel leakage in a frequency region of interest is the sum of the out-of-band-emissions from all frequency segments used by the wide-band signal transmission.

Consider a target spectrum segment with available bandwidth  $2f_A$ , i.e. valid signal frequency  $f \in [f_c - f_A, f_c + f_A]$  where  $f_c$  is the center frequency of the spectrum segment (relative to the center frequency of the wide-band system). In theory, the spectrum segment allows signal transmission at a maximum symbol rate  $2f_A$ . The actual symbol rate  $2f_B$  is usually less than  $2f_A$  with  $f_A - f_B$  being the size of the guard bands at each side of the spectrum.

Baseband pulse shaping is used to limit the frequency extent of the transmitted signal. The transmitted time-

domain baseband signal  $s(t)$  can be expressed as:

$$s(t) = \sum_n x(n)h(t - nT_B) \quad (16)$$

Here  $x(n)$  is the  $n$ -th transmitted symbol value;  $h(t)$  is the shaping pulse; and  $T_B = 1/(2f_B)$  is the symbol period. The frequency-domain signal representation is:

$$S(f) = \sum_n x(n)H(f)e^{-j2\pi f(nT_B)} \quad (17)$$

where  $H(f)$  is the Fourier transform of  $h(t)$ . The normalized signal power spectrum is

$$\begin{aligned} I(f) &= \frac{1}{(\sum_n 1)} E[|S(f)|^2] \\ &= |H(f)|^2 \end{aligned} \quad (18)$$

where we have assumed the symbol value  $x(n)$ s are independent with unit power, i.e.

$$E[x(n)x^*(m)] = \delta(n - m)$$

In practice,  $h(t)$  often takes the form of a square root raised cosine (SQRT RC) filter – such that inter-symbol-interference-free (ISI-free) reception can be achieved by applying a matched SQRT RC filter on the received signal. In this case, the frequency-domain filter response  $H(f)$  is a square root raised cosine window and  $|H(f)|^2$  is a raised cosine window:

$$\begin{aligned} &|H(f)|^2 \\ &= \begin{cases} \frac{1}{2} + \frac{1}{2} \cos \frac{\pi \left[ \frac{f}{2f_B} + \frac{1-\beta_H}{2} \right]}{\beta_H} & \frac{f}{2f_B} \in \left[ -\frac{1+\beta_H}{2}, -\frac{1-\beta_H}{2} \right] \\ 1 & \frac{f}{2f_B} \in \left[ -\frac{1-\beta_H}{2}, \frac{1-\beta_H}{2} \right] \\ \frac{1}{2} + \frac{1}{2} \cos \frac{\pi \left[ \frac{f}{2f_B} - \frac{1-\beta_H}{2} \right]}{\beta_H} & \frac{f}{2f_B} \in \left[ \frac{1-\beta_H}{2}, \frac{1+\beta_H}{2} \right] \\ 0 & \text{Otherwise} \end{cases} \end{aligned} \quad (19)$$

Since  $H(f)$  has finite frequency extent,  $h(t)$  has infinite time extent. In any practical implementation, a truncated version of  $h(t)$  must be used. Suppose such truncation is achieved through a time-limiting window  $w(t)$ , i.e.

$$h_W(t) = h(t)w(t) \quad (20)$$

where  $h_W(t)$  is the truncated version of  $h(t)$ . The normalized power spectrum (18) becomes:

$$I(f) = |H_W(f)|^2 = |H(f) \otimes W(f)|^2 \quad (21)$$

We choose  $w(t)$  to be a raised cosine window with window width  $T_W$  and roll-off factor  $\beta_W$ , which defaults

to a rectangular window when  $\beta_W = 0$ . The frequency domain response of the truncation window is then:

$$W(f) = \frac{\sin(\pi f T_W) \cos(\pi \beta_W f T_W)}{\pi f (1 - 4\beta_W^2 f^2 T_W^2)} \quad (22)$$

We defined the normalized ACL as:

$$\gamma_{\text{ACL}} = \frac{\int_{f > |f_A|} I(f) df}{\int_{f \leq |f_A|} I(f) df} = \frac{\int_{-\infty}^{\infty} I(f) df - \int_{-f_A}^{f_A} I(f) df}{\int_{-f_A}^{f_A} I(f) df} \quad (23)$$

where the signal power spectrum  $I(f)$  is given by (21).

$\gamma_{\text{ACL}}$  depends on the following parameters:

- Normalized guard band size  $1 - f_B/f_A$ , or equivalently normalized data rate  $f_B/f_A$ .
- Pulse shaping filter roll-off  $\beta_H$ , if SQRT RC filter is used for pulse shaping.
- Normalized truncation window width  $T_W/T_B$ .
- Truncation window roll-off  $\beta_W$ , if RC window is used for truncation.

Simulations were performed to explore the parameter dependencies of  $\gamma_{\text{ACL}}$ . Figure 4 shows the simulated  $\gamma_{\text{ACL}}$  dB contours over different  $\beta_H$ s and  $\beta_W$ s when the normalized data rate is fixed at 0.8 (normalized guard band size 0.2) and truncation window width  $T_W/T_B$  at 10. Note that when  $\beta_H$  is bigger than the guard size, e.g. when  $\beta_H = 0.3$ , the ACL is significant and depends almost solely on  $\beta_H$ , since in this case the pulse shaping filter bandwidth is larger than the available bandwidth  $2f_A$ . With  $\beta_H$  decreasing, the ACL becomes smaller until it hits a minimum when the pulse shaping filter bandwidth is close to the available bandwidth  $2f_A$ . For a fixed truncation window, further decrease in  $\beta_H$  increases ACL, because smaller pulse shaping filter roll-off  $\beta_H$  produces a larger time-domain signal tail that is cut off by the truncation window, resulting in increased ACL in frequency domain.

If the truncation window roll-off is fixed, by varying the truncation window width  $T_W/T_B$  and the pulse shaping filter roll-off  $\beta_H$ , we obtain the ACL contours shown in Figure 5, where  $\beta_W = 0.25$ . As long as the pulse shaping filter bandwidth is smaller than the available bandwidth, a bigger truncation window means a larger portion of the time-domain pulse shaping filter signal tail will be retained after windowing resulting in reduced ACL in frequency domain. Using a larger window roll-off  $\beta_W$  will improve the ACL performance further. Figure 6 shows the ACL contours when window roll-off  $\beta_W = 0.75$ .

The simulation results show that excellent adjacent channel leakage performance can be achieved using a

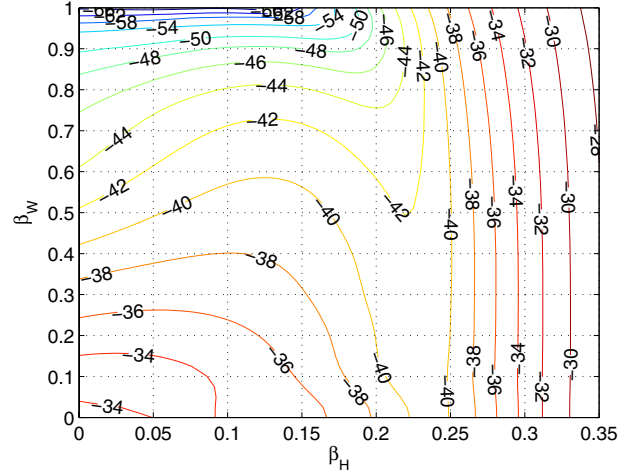


Fig. 4. Simulated adjacent channel leakage dB contours for normalized data rate  $f_B/f_A = 0.8$  and normalized truncation window width  $T_W/T_B = 10$ .

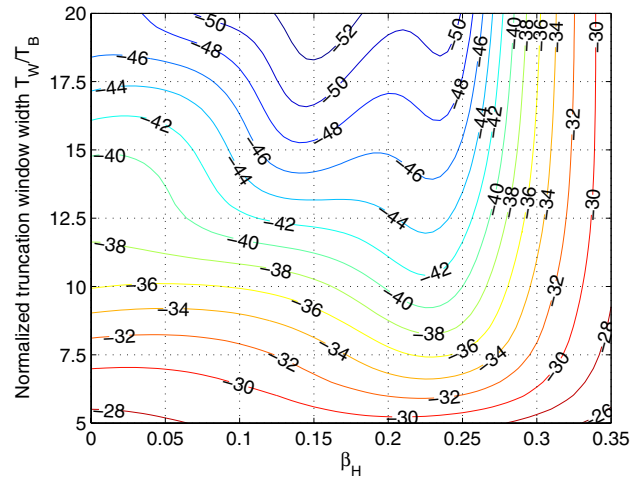


Fig. 5. Simulated adjacent channel leakage dB contours for normalized data rate  $f_B/f_A = 0.8$  and truncation window roll-off  $\beta_W = 0.25$ .

proper set of system parameters. Note that the truncation window width directly relates to the filter implementation complexity. For example, if  $T_W/T_B = 10$  and if the wide-band system fundamental sampling period is  $T_s = T_B/20$ , the truncated pulse shaping filter would have at least 200 taps. Note further that we have only considered ACL here. Truncation may also increase ISI which may be considered together with the ACL when analyzing system performance tradeoffs.

2) *Frequency-domain signal, OFDM:* For frequency-domain signal like OFDM, the corresponding time-

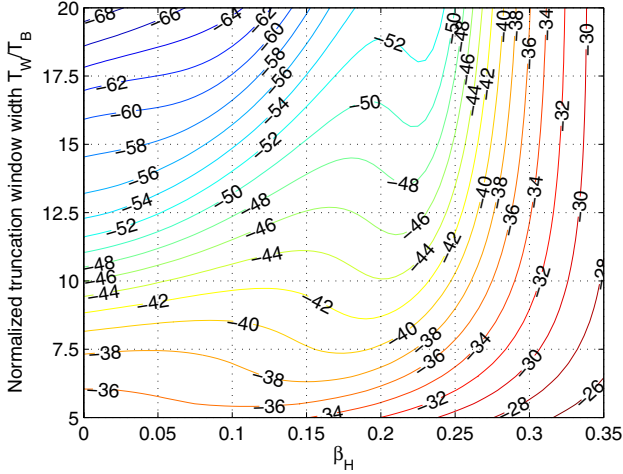


Fig. 6. Simulated adjacent channel leakage dB contours for normalized data rate  $f_B/f_A = 0.8$  and truncation window roll-off  $\beta_W = 0.75$ .

domain signal waveform is truncated to create an OFDM symbol. Such truncation is necessary in order to limit the extent of the time-domain OFDM signal waveform so that multiple OFDM symbols can be time-multiplexed to create an OFDM packet. OFDM symbol truncation is achieved through time-domain windowing. A typical symbol window is an RC window. Just as discussed before for the time-domain signals, time-domain truncation through windowing creates adjacent channel leakage in frequency domain. Window parameters must be carefully chosen to minimize the ACL.

We assume an RC window  $w(t)$  with width  $T_W$  and roll-off  $\beta_W$  is used as the OFDM symbol window. We write the time-domain OFDM signal as:

$$s(t) = \sum_n \left[ w(t - nT_W) \sum_{k \in \Omega} X(n, k) e^{j2\pi \frac{k}{T}(t - nT_W)} \right] \quad (24)$$

Here  $n$  is the OFDM symbol index;  $k$  is the subchannel index;  $\Omega$  is the collection of data subchannels (in the unused spectrum segments);  $X(n, k)$  is the transmitted signal value on symbol  $n$  subchannel  $k$ ; and  $T$  is the FFT symbol period.

Note that the OFDM symbol window width  $T_W$  is larger than the FFT symbol period  $T$ . The extra  $T_G = T_W - T$  portion of the windowed OFDM symbol, which is cyclically extended from the FFT symbol, is used as a guard period against multipath delay spread. Note further that to ensure there is no inter-carrier-interference (ICI), the window must be flat over the FFT symbol region,

indicating  $(1 - \beta_W)T_W > T$ .

The frequency-domain representation of the signal is:

$$S(f) = \sum_n \sum_{k \in \Omega} X(n, k) W\left(f - \frac{k}{T}\right) e^{-j2\pi f(nT_W)} \quad (25)$$

where  $W(f)$  is the Fourier transform of  $w(t)$ , given by (22). The normalized signal power spectrum is:

$$\begin{aligned} I(f) &= \frac{1}{(\sum_n 1)} E[|S(f)|^2] \\ &= \sum_{k \in \Omega} \left| W\left(f - \frac{k}{T}\right) \right|^2 \end{aligned} \quad (26)$$

where in deriving the second equality, we have assumed  $X(n, k)$ s are independent with unit power, i.e.

$$E[X(n, k)X^*(m, l)] = \delta(n - m)\delta(k - l)$$

As discussed before, we will again focus on the out-of-band emission from a particular spectrum segment with available bandwidth  $2f_A$ . The data bandwidth is  $2f_B$  and the total guard band size is  $2f_A - 2f_B$ . The normalized adjacent channel leakage  $\gamma_{ACL}$  is again defined by Equation (23) with  $I(f)$  given by (26) and  $W(f)$  given by (22). For OFDM,  $\gamma_{ACL}$  depends on the following parameters:

- Normalized guard band size  $1 - f_B/f_A$ .
- Subchannel spacing  $1/T$ , or equivalently the number of data subchannels  $N = 2f_B T$ , given fixed data bandwidth  $2f_B$ .
- OFDM symbol window width  $T_W/T$  (normalized to the FFT symbol period).
- OFDM symbol window roll-off  $\beta_W$ .

Simulations were performed to explore the parameter dependencies of the ACL. Figure 7 shows the simulated  $\gamma_{ACL}$  dB contours over different  $T_W/T$ s and  $\beta_W$ s, at normalized guard band size  $1 - f_B/f_A = 0.1$  and number of subchannels  $N = 2f_B T = 32$ . Only some combinations of  $T_W/T$  and  $\beta_W$  are valid if we recall the requirement that  $(1 - \beta_W)T_W > T$  to ensure ICI-free operation. The improved ACL performance is shown in Figure 8 when the guard band size is increased to 0.2. Figure 9 shows the dependencies of the ACL on the number of data subchannels  $N = 2f_B T$  (or subchannel spacing  $1/T$ ) and the symbol window roll-off  $\beta_W$ , at normalized guard band size of 0.2 and symbol window width  $T_W/T = 1.5$ . The simulation results show that excellent ACL performance can be achieved by OFDM-based wide-band cognitive radio systems if proper system parameters are chosen.

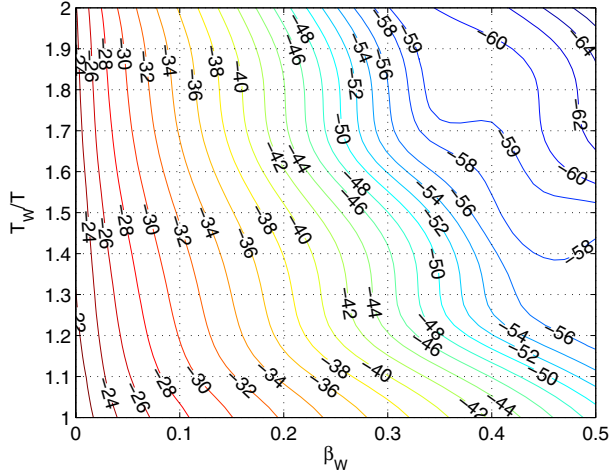


Fig. 7. Simulated OFDM system adjacent channel leakage dB contours for normalized data bandwidth  $f_B/f_A = 0.9$  and number of data subchannels  $N = 32$ .

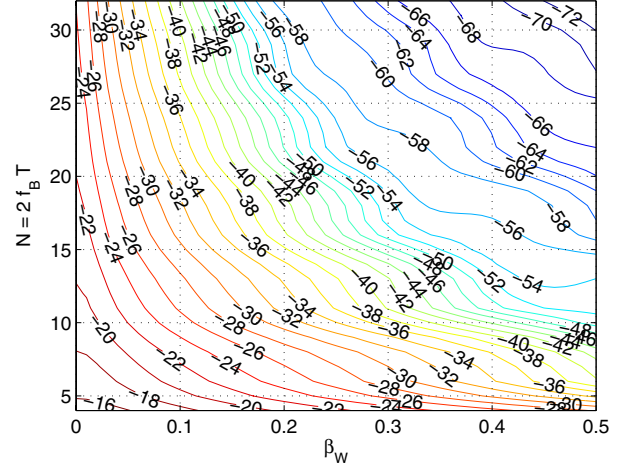


Fig. 9. Simulated OFDM system adjacent channel leakage dB contours for normalized data bandwidth  $f_B/f_A = 0.8$  and symbol window width  $T_W/T = 1.5$ .

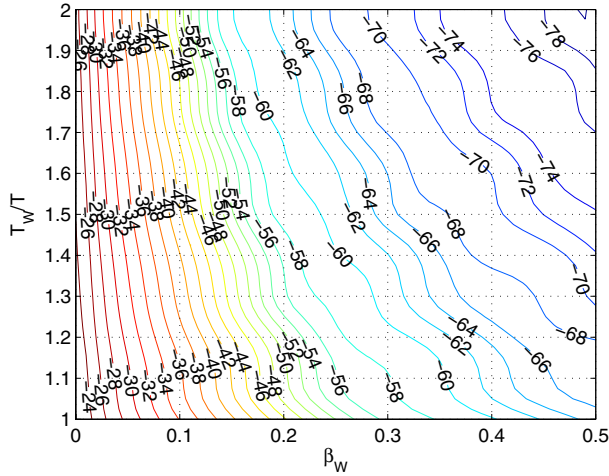


Fig. 8. Simulated OFDM system adjacent channel leakage dB contours for normalized data bandwidth  $f_B/f_A = 0.8$  and number of data subchannels  $N = 32$ .

### B. Transmission nonlinearity

In addition to signal time-domain truncation, another ACL mechanism is transmission nonlinearity due to cascaded nonlinear components in the RF transmitter chain. We will briefly discuss such mechanism in the context of this paper and interested reader may find in-depth treatment of the topic elsewhere [10].

While all nonlinear elements in the RF transmitter chain contribute to the transmission nonlinearity, in practice, the nonlinearity is often dominated by the nonlinearity of the power amplifier (PA) which performs

the last-stage amplification in the transmitter chain. The transmission nonlinearity can usually be modeled using the nonlinear transfer function:

$$y(t) = \alpha_1 x(t) + \alpha_2 x^2(t) + \alpha_3 x^3(t) + \dots \quad (27)$$

where  $x(t)$  is the input signal to the transmitter chain;  $y(t)$  is the output signal from the transmitter chain; and  $\alpha_1, \alpha_2, \dots$  are the nonlinear coefficients of the transmitter chain.

Small-signal nonlinearity is usually dominated by the low-order nonlinear terms. Furthermore, for passband signals with proper filtering, the even-order nonlinear terms are usually negligible. The odd-order nonlinear terms, however, are responsible for generating intermodulation products that can cause in-band and adjacent-band interferences. In view of the above, the nonlinear transfer function (27) is often approximated as:

$$y(t) = \alpha_1 x(t) + \alpha_3 x^3(t) \quad (28)$$

The nonlinearity of the above transfer function is measured by a single parameter – the third-order interception point (IP3) – defined as:

$$\text{IP3 (dB)} = 10 \log_{10} \alpha_1^3 - 10 \log_{10} \frac{3\alpha_3}{4} \quad (29)$$

Given certain output signal power from the transmitter, the (dB) difference between the output signal level and the ACL due to transmission nonlinearity is approximately twice the (dB) difference between the overall transmitter chain IP3 and the output signal level [11].

High linearity (or equivalently high IP3) is usually required for cognitive radio transmitters to ensure minimal interference to the primary users. However, high linearity transmitter chain is not only more expensive but also less power efficient. One way to reduce the IP3 requirement is to use pre-distortion techniques. A pre-distortion module pre-compensates the signal entering a nonlinear device for anticipated distortion so that the output from the combined pre-distortion module and the nonlinear device is undistorted. Effective pre-distortion can be achieved through both analog and digital means as discussed in [10].

## V. CONCLUSION

In this paper, we investigated some fundamental physical layer issues of wide-band cognitive radio systems. We argue that OFDM is the best physical layer candidate for wide-band cognitive radio systems because it allows easy generation of spectral signal waveforms that can fit into discontinuous and arbitrary-sized spectrum segments. OFDM is also optimal from a capacity point of view since it allows achieving the Shannon channel capacity in a fragmented spectrum.

A cognitive radio identifies unused spectrum segments in a target primary user spectrum through spectrum sensing. We have separated physical layer sensing methods into two categories: power-based sensing methods and waveform-based sensing methods. While power-based sensing is more general, waveform-based sensing outperforms power-based sensing in reliability and sensing convergence time. Waveform-based sensing, however, is only possible when the target primary user signal contains known signal patterns.

Using central limit theorem, we have analyzed the performances of the generalized power-based sensing and waveform-based sensing. In each case, the performance is characterized by the sensing error floor (SEF), defined as either the sensing false detection probability or the sensing loss detection probability when the two are equal. Closed-form SEFs have been derived and simulated. Power-based sensing and waveform-based sensing exhibit similar performances at high SNR. Power-based sensing, however, works poorly at low SNR, when its sensing convergence time increases quadratically with the SNR reduction, comparing to waveform-based sensing, whose sensing convergence time increases linearly with the SNR reduction. We argue that a combination of power-based sensing, waveform-based sensing, and network-layer sensing collaboration [9] may be needed in a practical shadowing environment.

To ensure successful operation, a cognitive radio must minimize the interference to the primary user bands by reducing the adjacent channel leakage (ACL). We have identified two ACL mechanisms: signal time-domain truncation and transmission nonlinearity.

ACL due to signal time-domain truncation is inevitable but it can be controlled through proper system parameter choices. For time-domain signals, the parameters affecting ACL include: guard band size, pulse shaping filter roll-off, truncation window width, and truncation window roll-off. For OFDM, the parameters affecting ACL include: guard band size, subchannel spacing, OFDM symbol window width, and OFDM symbol window roll-off. Adjacent channel leakage analyses were conducted for both cases. Simulations were performed to determine ACL parameter dependencies. The simulation results demonstrate that excellent ACL performances can be achieved for both cases when proper sets of system parameters are used.

Finally, we briefly discussed the ACL due to transmission nonlinearity, which depends on the transmitter output power level and the overall transmitter chain IP3. To ensure minimal interference, high linearity is required for cognitive radio transmitters, which may be achieved through analog and digital pre-distortion techniques [10].

## REFERENCES

- [1] SPTF, "Report of the spectrum efficiency working group," November 2002.
- [2] J. Mitola, "Cognitive radio for flexible mobile multimedia communications," *Mobile Networks and Applications*, vol. 6, September 2001.
- [3] FCC, "Facilitating opportunities for flexible, efficient, and reliable spectrum use employing cognitive radio technologies," *ET Docket No. 03-108*, December 2003.
- [4] <http://www.darpa.mil/ato/programs/xg/>
- [5] FCC, "Fcc first report and order: Revision of part 15 of the commission's rules regarding ultra-wideband transmission systems," *ET Docket No. 98-153*, April 2002.
- [6] H. Tang, *A Unified Approach to Wireless System Design*. PhD thesis, University of California at Berkeley, 2002.
- [7] R. van Nee and R. Prasad, *OFDM for Wireless Multimedia Communications*. Artech House, 2000.
- [8] A. Leon-Garcia, *Probability and Random Processes for Electrical Engineering*. Addison Wesley, second ed., 1994.
- [9] Adaptrum, "Comments to fcc nprm et docket no. 04-186," September 2004.
- [10] F. H. Raab, "Power amplifiers and transmitters for rf and microwave," *IEEE Transactions on Microwave Theory and Techniques*, vol. 50, March 2002.
- [11] B. Razavi, *RF Microelectronics*. Pearson-Prentice Hall, 1998.